Enhancement of Galloping-based Wind Energy Harvesting by Synchronized Switching Interface Circuits

Liya Zhao[a], Junrui Liang[b], Lihua Tang[c]*, Yaowen Yang[a], Haili Liu[b]

[a]School of Civil and Environmental Engineering, Nanyang Technological University, 50 Nanyang Avenue, Singapore 639798; [b]School of Information Science and Technology, ShanghaiTech University, 319 Yueyang Road, Shanghai 200031, P.R. China; [c]Department of Mechanical Engineering, University of Auckland, 20 Symonds Street, Auckland 1010, New Zealand

ABSTRACT

Galloping phenomenon has attracted extensive research attention for small-scale wind energy harvesting. In the reported literature, the dynamics and harvested power of a galloping-based energy harvesting system are usually evaluated with a resistive AC load; these characteristics might shift when a practical harvesting interface circuit is connected for extracting useful DC power. In the family of piezoelectric energy harvesting interface circuits, synchronized switching harvesting on inductor (SSHI) has demonstrated its advantage for enhancing the harvested power from existing base vibrations. This paper investigates the harvesting capability of a galloping-based wind energy harvester using SSHI interfaces, with a focus on comparing the performances of Series SSHI (S-SSHI) and Parallel SSHI (P-SSHI) with that of a standard DC interface, in terms of power at various wind speeds. The prototyped galloping-based piezoelectric energy harvester (GPEH) comprises a piezoelectric cantilever attached with a square-sectioned bluff body made of foam. Equivalent circuit model (ECM) of the GPEH is established and system-level circuit simulations with SSHI and standard interfaces are performed and validated with wind tunnel tests. The benefits of SSHI compared to standard circuit become more significant when the wind speed gets higher; while SSHI circuits lose the benefits at small wind speeds. In both experiment and simulation, the superiority of P-SSHI is confirmed while S-SSHI demands further investigation. The power output is increased by 43.75% with P-SSHI compared to the standard circuit at a wind speed of 6m/s.

Keyword: galloping, energy harvesting, SSHI interface, piezoelectric, equivalent circuit model

1. INTRODUCTION

In the recent years, research on energy harvesting has flourished with the ultimate goal of totally replacing the life-limited batteries with energy harvesters to implement self-powered wireless sensor networks (WSNs). Piezoelectric transduction mechanism is one promising option to realize the conversion of the available kinetic energy in the ambient environment into electrical energy. Many studies have been conducted to investigate the performance of vibration-based piezoelectric energy harvesters [1-4]. Besides the pre-existing mechanical vibrations, the bulky kinetic energy in the wind flows is an alternative energy source. Harvesting wind energy using the piezoelectric materials has attracted many research interests in the recent years. Some designs of wind energy harvesters have taken forms of the traditional windmills via direct mechanical impact [5] or non-impact magnetic interactions [6] to induce oscillatory deformations of the piezoelectric elements. Many other designs have tried to induce vibrations of the piezoelectric structure via aeroelastic instabilities. Examples of such kinds of energy harvesters include those based on vortex-induced vibrations [7,8], galloping [9-15], aeroelastic flutter [16-18]. Energy harvesters that are designed to mimic the behavior of a harmonica [19] and the oscillations of grass in turbulent flows [20] have also been reported in the literature.

The piezoelectric energy harvesting process based on aeroelastic instabilities involves complex mutual interactions between the flowing fluid, mechanical structure, piezoelectric element, and the interface circuit connected to the piezoelectric elements. The power output of aeroelastic energy harvester is influenced simultaneously by the multiphysics dynamic behaviors, i.e., aero-electro-mechanical coupling. In order to enhance the performance of the aeroelastic energy harvesters, some techniques have been proposed from the mechanical aspects to modify the structural designs, like adding a movable mass to adjust the resonance frequency thus to broaden the functional wind speed range

*Author to whom correspondence should be addressed. Email: l.tang@auckland.ac.nz

Active and Passive Smart Structures and Integrated Systems 2015, edited by Wei-Hsin Liao,
Proc. of SPIE Vol. 9431, 94310E · © 2015 SPIE · CCC code:
0277-786X/15/$18 · doi: 10.1117/12.2084000

of a harvester based on vortex-induced vibrations [21], using a two degree-of-freedom of structure with magnetic interaction to enhance the output power of a galloping harvester in the low wind speed range [14], integrating the base vibratory excitation with the aerodynamic forces for performance improvement [15,18], and adding a beam stiffener to amplify the electromechanical coupling thus to increase the power extraction efficiency of the aeroelastic energy harvesters [22]. From the aspect of interface circuits, researches have mostly simplified the circuit as a pure resistor to ease the analysis of the aforementioned complex mutual coupling behaviors, although the power enhancing capabilities of optimized nonlinear interfaces have been widely confirmed in the base-excited vibration energy harvesting [23-29]. Several studies have considered employing nonlinear interface circuits in aeroelastic energy harvesting [30-33]. It was determined by Zhao et al. [32,33] that the output power of a galloping based energy harvester can be greatly enhanced by the synchronized charge extraction (SCE) interface circuit compared to that with a standard circuit, when the electromechanical coupling is less than a critical coupling limit. It was also found that the critical coupling, thus the applicable region of the SCE circuit, increases with the wind speed.

Using a self-powered S-SSHI circuit, Liang and Liao [29] have experimentally and analytically proved that the power of a conventional vibration energy harvester can be boosted up to 200% more than that with the standard circuit. In this paper, we investigate the energy harvesting capability of a GPEH using the SSHI circuits. The performances of S-SSHI and P-SSHI are compared with that of a standard circuit, with a focus on the power output at various wind speeds. Wind tunnel experiment is conducted to verify the equivalent circuit simulation results.

2. GPEH SYSTEM

2.1 Configuration of GPEH

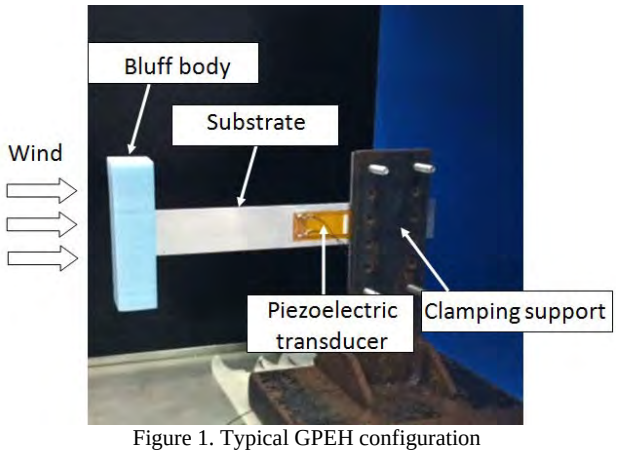

Figure 1. Typical GPEH configuration

Figure 1 shows a typical configuration of a GPEH consisting of a square-sectioned bluff body attached to the free end of a cantilever [12]. A piece of piezoelectric patch is bonded to the fixed area where the largest strain occurs during vibration. The system is controlled by the nonlinear damping under the aerodynamic galloping force, which is resulted from the fluid-structure interaction between the wind flow and the square bluff body. When the wind speed U surpasses a critical value, i.e., the cut-in wind speed U_{cr}, the bluff body will undergo limit cycle oscillation in the direction normal to the wind flow, which causes alternating strain in the piezoelectric patch. AC electrical output is then generated via direct piezoelectric effect. The AC output requires further rectification and regulation before being realistically used for energy storage or DC power supply for electronic devices.

2.2 Analytical model of GPEH system:

$$\ddot{\eta}(t)+2\zeta\omega_n\dot{\eta}(t)+\omega_n{}^2\eta(t)+\chi V_p(t)=f_{galloping}(t) \tag{1}$$

$$I(t)+C_p\dot{V}_p(t)-\chi\dot{\eta}(t)=0 \tag{2}$$

$$f_{galloping}(t)=\phi(L_t)\times\frac{1}{2}\rho hlU^2\sum_{i=1}^{3}A_i\left[\frac{\phi(L_t)\dot{\eta}(t)}{U}+\phi'(L_t)\eta(t)\right]^i \tag{3}$$

Analytical aero-electro-mechanical model of a GPEH system includes two parts: the electromechanical model and the aerodynamic model. The electromechanical model consists of the equation of motion given in Equation (1) and the circuit model shown in Equation (2), where $\eta(t)$, ζ and ω_n are the modal coordinate, mechanical damping ratio and undamped fundamental frequency of the first vibration mode, respectively; C_p is the capacitance of the piezoelectric patch; $V_p(t)$ is the voltage across the piezoelectric patch; $I(t)$ is the current flow into the interface circuit; and χ is the modal electromechanical coupling term. χ is further related to another coupling term, which is defined by the geometric and material properties of the composite beam cross section, and the slope change of the fundamental mode shape ϕ of the beam at the two edges of the piezoelectric patch [10,13,22]. The modal aerodynamic force $f_{galloping}$ is expressed in Equation (3), where U, A_i, L_t, ρ, h and l are the wind speed, empirical aerodynamic coefficients, length of the cantilever, air density, frontal dimension and length of the bluff body, respectively. For detailed derivation, readers are referred to the work of Sirohi and Mahadik [9], Abdelkefi et al. [10] and Zhao et al. [13].

3. INTERFACE CIRCUITS

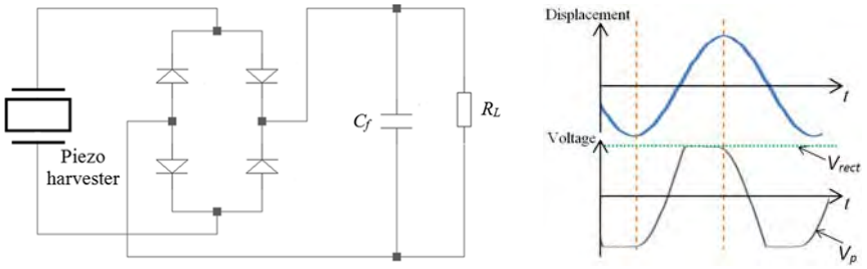

(a) (b)

Figure 2. (a) Standard interface circuit and (b) waveforms of voltage and tip displacement

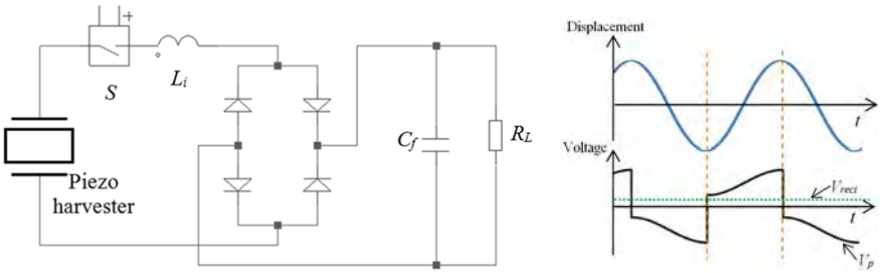

(a) (b)

Figure 3. (a) S-SSHI interface circuit and (b) waveforms of voltage and tip displacement

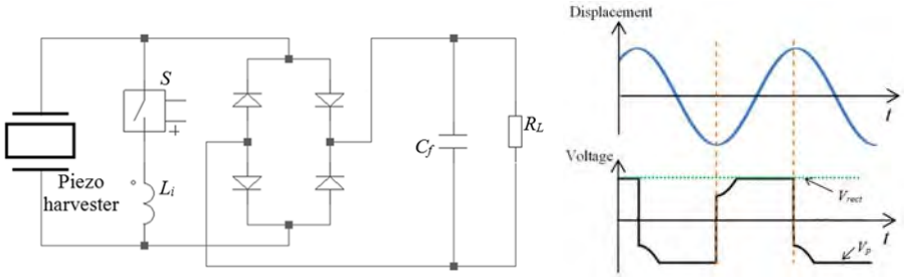

(a) (b)

Figure 4. (a) P-SSHI interface circuit and (b) waveforms of voltage and tip displacement

Three types of interfaces are considered in this paper, i.e., the standard DC interface shown in Figure 2, the S-SSHI interface shown in Figure 3 and the P-SSHI interface shown in Figure 4. The standard circuit includes a full-wave rectifier to convert AC to DC and a filtering capacitor C_f to smooth the voltage V_{rect} across the terminal load R_L. V_{rect} is safe to be considered constant when C_f is chosen to be large. A drawback of the standard circuit is that during a certain interval in each cycle of vibration, the energy is returned back from the electrical part to the mechanical part, restraining

the efficiency of power extraction. This issue can be overcome in the SSHI circuit by adding an inductive switch path to enhance the nonlinear power extraction process. The inductive switch path consisting of a switch S and an inductor L_i is connected in series to the bridge rectifier in S-SSHI (Figure 3(a)) and in parallel in P-SSHI (Figure 4(a)). Regardless of the series or parallel connection, S is triggered on once the transverse displacement of the bluff body reaches its extreme values to form an S-L_i-C_p loop with the piezoelectric element. Then S is triggered off after half of the oscillating period of the loop to complete a natural inversion of the piezoelectric voltage V_p [29]. Typical waveforms of the three interface circuits are also given in Figures 2, 3 and 4.

4. EQUIVALENT CIRCUIT MODELING OF GPEH

Connecting a nonlinear interface circuit involves further complexity in the system which has already processed complex mutual interactions between the flowing fluid, mechanical structure and piezoelectric element as mentioned above. Formulation for the responses of the more sophisticated three-way coupling behaviors will become quite cumbersome. Therefore, some researchers have proposed to represent the aeroelastic energy harvester with an equivalent circuit model (ECM) [34,35] to enable system level circuit simulation integrating the mechanical structure of the harvester and the aerodynamic force with the nonlinear power extraction interface. The ECM employed in this paper is shown in Figure 5. It was established based on the parameter analogies between the mechanical domain and the electric domain and a non-standard component representing the aerodynamic force due to galloping. For detailed derivation process readers are referred to Tang et al. [34]. This ECM has been validated via wind tunnel experiment and a successful example of its integration with an SCE interface for system-level circuit simulation of a galloping harvester can be found in Zhao et al. [32,33]. The values of the components in Figure 5 are identified from the physical, mechanical and electromechanical properties of the GPEH prototypes (details in Zhao et al. [32,33]).

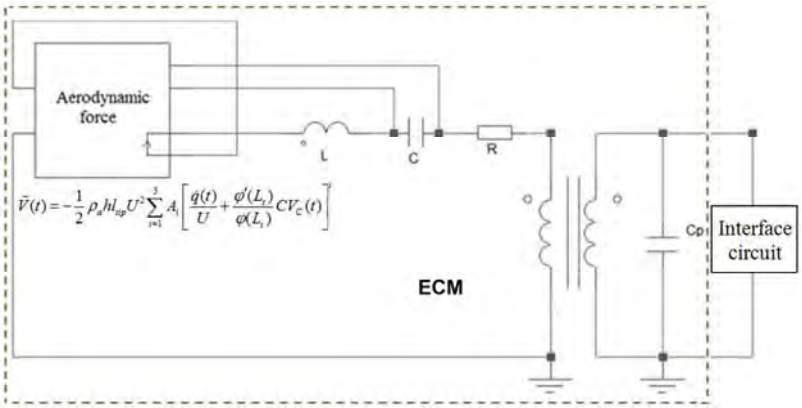

Figure 5. ECM of GPEH

Table 1. Properties of the GPEH prototype

Properties	Cantilever	
	Substrate beam	Piezoelectric sheet
Length L_t, L_p(mm)	130	28
Width b_s, b_p(mm)	20	14
Thickness h_s, h_p(mm)	0.6	0.3
Material	Aluminum	MFC M2814-P2
Mass Density (kg m^{-3})	2700	5440
Capacitance C_p(nF)	--	25.7
Young's Modulus E_s, E_p (GPa)	69	30.336
	Bluff body	
Mass M_{tip}(kg)	0.0018	
Length l (mm)	100	
Cross section h×h (mm)	20×20	
Aerodynamic coefficients A_1, A_2, A_3	2.3, 0, -18	

5. EXPERIMENT AND CIRCUIT SIMULATION

5.1 Experiment

5.1.1 Prototype of GPEH and circuit hardware

Wind tunnel experiment with a fabricated GPEH prototype and a built up circuit hardware is carried out to evaluate the wind power extraction performance of the GPEH integrated with SSHI. The piezoelectric patch used is MFC M2814-P2 (Smart Materials Corp.). The air density, ζ and short circuit fundamental frequency is 1.204kg/m^3, 0.011 and 16.67Hz, respectively. Other properties of the GPEH prototype are listed in Table 1.

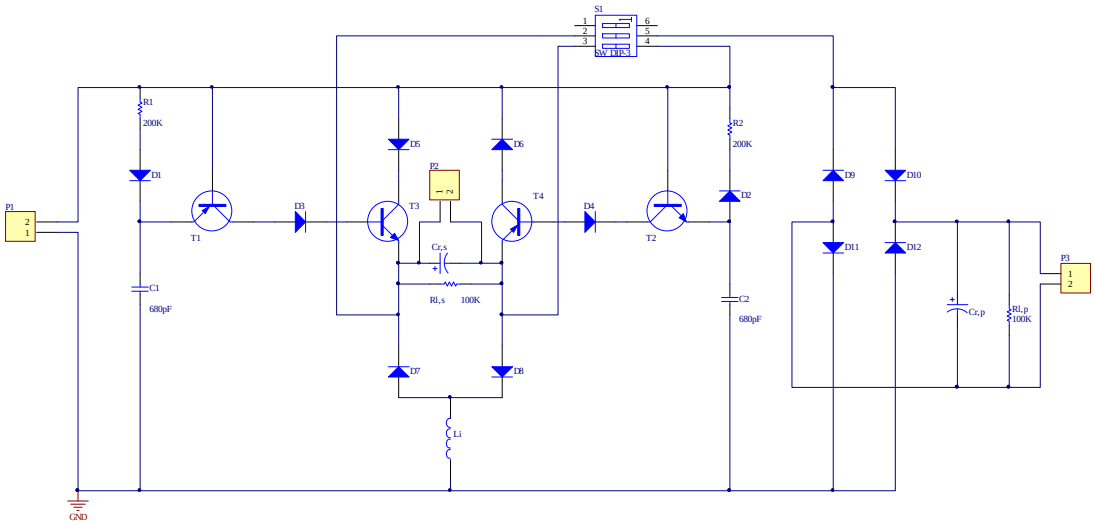

Figure 6. Schematic of the built-up self-powered S-SSHI and P-SSHI circuit hardware

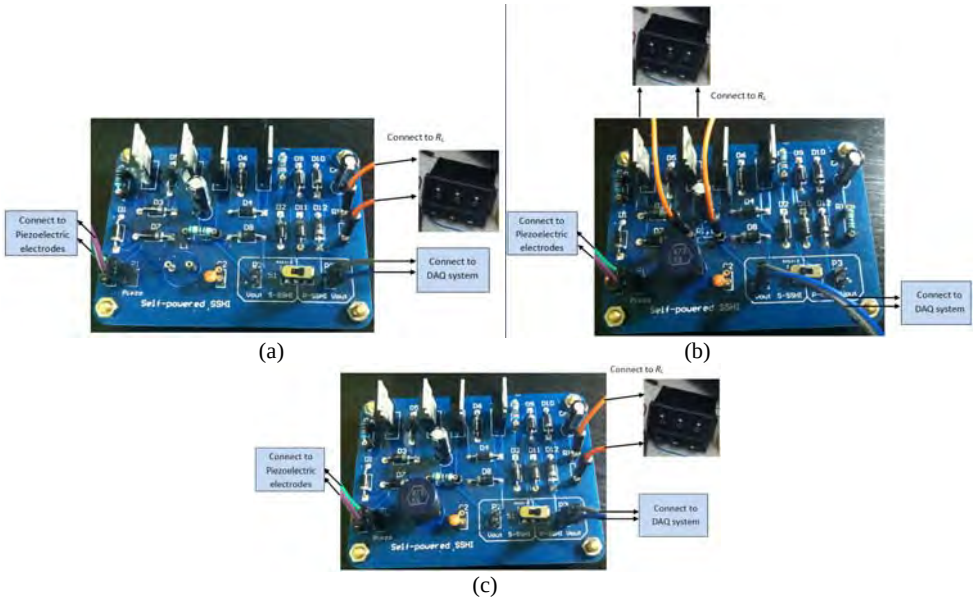

Figure 7. Hardware configuration for (a) the standard circuit (b) self-powered S-SSHI circuit and (c) self-powered P-SSHI circuit.

A circuit hardware is built up and connected to the GPEH prototype for the wind tunnel test. The schematic for the circuit hardware is shown in Figure 6. By changing the connection with the DIP switch, it can work as a self-powered S-SSHI, self-powered P-SSHI. Removing the inductor L_i in P-SSHI configuration, it can work as the standard circuit as

well. In the self-powered SSHI configurations, electronic breakers composed of the envelope detector, comparator and switch are used to automatically detect the displacement extremes and perform switching actions, avoiding the requirement of an external displacement sensor and a switch controller. Both maximum and minimum electronic breakers are included. The improved design of electronic breaker with complementary transistors topology is employed here, which is proposed by Liang and Liao [29]. With this design, all the isolating resistors in the breaker in Richard et al. [36] and Lallart and Guyomar [26] that consume some harvested energy can be removed. The detailed working principles and analysis of the employed self-powered SSHI circuit are provided in Liang and Liao [29]. In Table 2, the load resistances r represent the total equivalent series resistance of the non-ideal switching path, of which the values for S-SSHI and P-SSHI are obtained by measuring the respective reference voltages at the instant of the first voltage inversion.

Table 2. Circuit component values

R_1 and R_2 (kΩ)	200
C_1 and C_2 (pF)	680
Diodes (D_1 to D_{12})	1N4004
PNP transistors (T_1 and T_4)	TIP32C
NNP transistors (T_2 and T_3)	TIP31C
C_f (μF)	20
L_i (mH)	47
S-SSHI, r(Ω)	252.4
P-SSHI, r(Ω)	283.0

5.1.2 Overall Experiment Setup in Wind Tunnel

Figure 8 shows the entire wind tunnel experiment setup. The voltage signal across the piezoelectric patch and the terminal load R_L is measured by the NI 9229 data acquisition module (National Instruments). The wind speed is measured with a hotwire anemometer.

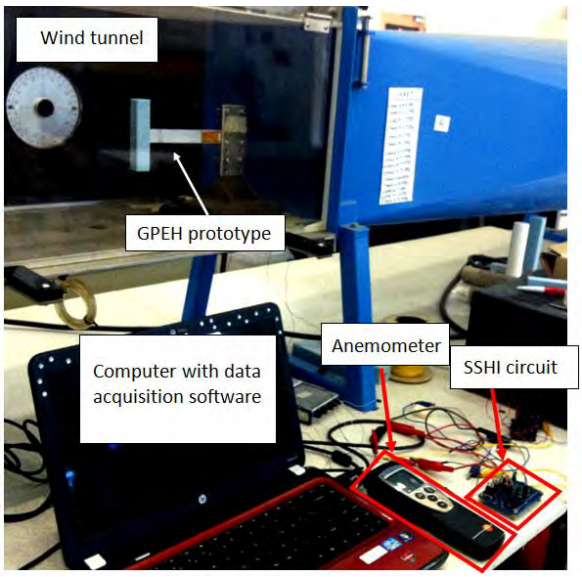

Figure 8. Overall experiment setup in the wind tunnel

5.2 Circuit Simulation

The overall circuit diagram for system-level circuit simulation consists of the equivalent circuit model of GPEH in Figure 5 integrated separately with the standard, S-SSHI and P-SSHI in Figure 6. By making sure the fundamental oscillation period of the harvester is much larger than the resonant period of the *LC* circuit, the voltage inversion can be regarded to happen instantly. The entire GPEH system with the integrated interfaces is simulated in the circuit simulator SIMetrix. A differential voltage probe is used in the simulation to obtain the voltage V_{rect} across R_L. The output power is calculated by $P=(V_{rect})^2/R_L$.

6. RESULTS AND DISCUSSION

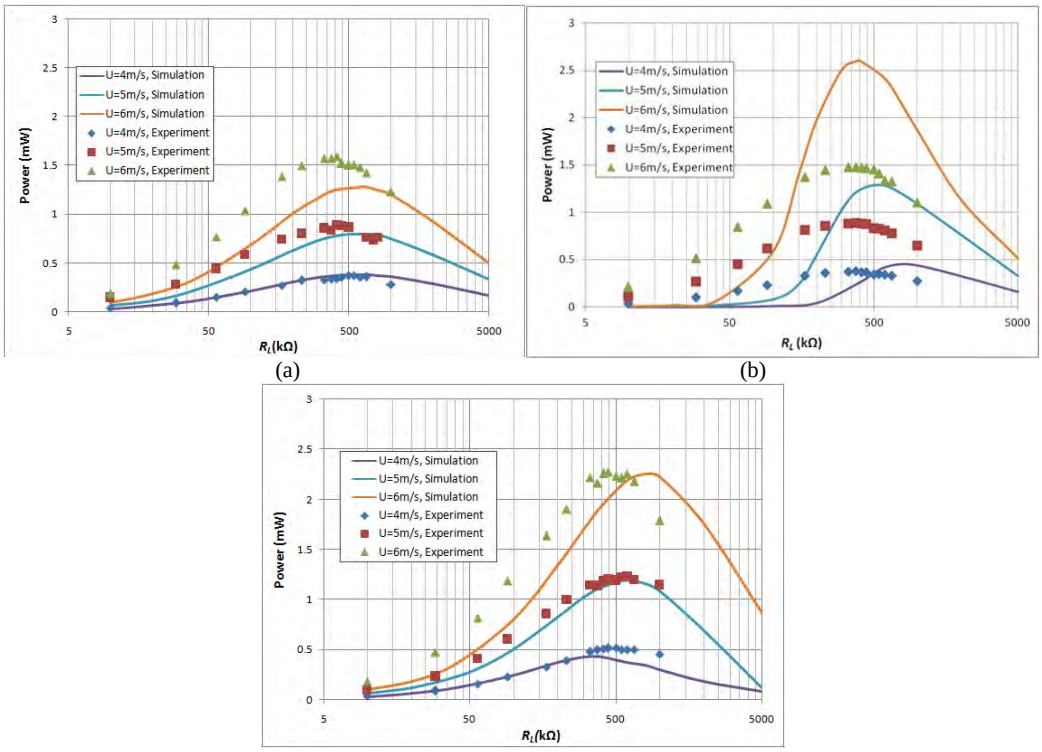

Figure 9. Measured and predicted output power versus terminal load at 4m/s, 5m/s and 6m/s. (a) Standard circuit (b) S-SSHI circuit (c) P-SSHI circuit.

Under three different wind speeds of U=4m/s, 5m/s and 6m/s, the measured and predicted variations of average power as a function of load resistance for the standard, S-SSHI and P-SSHI interfaces are compared in Figure 9. Comparing the amplitudes of the power from experimental results, it is observed that for all three circuits, the power increases with the wind speed, and P-SSHI gives the highest output power, with great enhancement compared to that with the standard circuit especially when the wind speed is high, e.g., at 6m/s the power is increased from 1.6mW with the standard circuit into 2.3mW with P-SSHI in the experiment, corresponding to a 43.75% increase. Enhancement is also predicted for S-SSHI by circuit simulation, yet is not reflected by the experimental results. In general, for standard and P-SSHI, the simulation results agree well with the wind tunnel test measurements. While for S-SSHI, discrepancy is significant for 6m/s and results at small R_L. It is found that at small R_L conditions, the circuit simulation for S-SSHI is not able to properly start up with C_1=C_2=680pF. Though not shown here, it is found in simulation that with the increase of C_1 and C_2, the discrepancy will be lessened (both power outputs at small R_L and the maximal power will get closer to the experimental measurements). The reason for this needs further investigation.

In addition, there exist an optimal resistance $R_{optimal}$ for maximum output power for all three circuits. With the variation of the wind speed, the value of $R_{optimal}$ keeps constant for the standard circuit (actually $R_{optimal}$ should be very slightly increased with the wind speed since the vibration frequency is slightly decreased when U is increasing according to the theoretical response solutions). However, $R_{optimal}$ varies greatly for S-SSHI and P-SSHI at different wind speeds, which is more obviously observed from the simulation. When wind speed increases within the considered range of U=4m/s~6m/s, the predicted $R_{optimal}$ decreases from 600kΩ to 300kΩ for S-SSHI, while $R_{optimal}$ for P-SSHI increases from 400kΩ to 800kΩ.

Based on the measured responses, the respective R_L that gives relative high output power for all three wind speeds (4m/s~6m/s) is chosen for each circuit, and then used to investigate the response of power versus wind speed, as shown in Figure 10. Values of R_L used for each circuit are: R_L=412kΩ for the standard circuit, R_L=375kΩ for S-SSHI and R_L=445kΩ for P-SSHI. For P-SSHI, both experiment and simulation results show enhancement of output power

compared to the standard circuit, with the degree of enhancement gets larger at higher wind speeds; while for S-SSHI, only circuit simulation captures the power enhancement, yet the experimental results are more or less comparative with those for standard circuit. This implies that a great energy loss occurs in the hardware S-SSHI which has not been successfully taken into account.

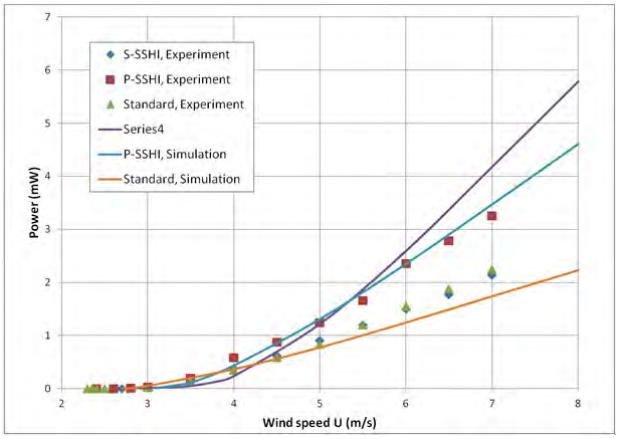

Figure 10. Measured and predicted power versus wind speed, with R_L=412kΩ for the standard circuit, R_L=375kΩ for S-SSHI and R_L=445kΩ for P-SSHI.

Inspecting the simulation responses, a general trend of power from the three circuits are observed at relatively high wind speeds, i.e., S-SSHI>P-SSHI>Standard. Moreover, the benefits of SSHI become more significant when the wind speed gets higher. At small wind speeds (below 3.8m/s), although not captured by experiment, the SSHI circuits lose their benefit compared to the standard circuit. These two issues are similar to the vibration based energy harvester as concluded in Liang and Liao [29]. Moreover, as aforementioned, it is observed during simulation that the output power of S-SSHI is sensitive to the values of the capacitors C_1 and C_2. The reason for discrepancy and the energy loss in S-SSHI deserves further investigations.

7. CONCLUSION

This paper investigates the energy harvesting capability of a galloping-based wind energy harvester using SSHI interfaces and compares the performance of S-SSHI and P-SSHI with that of a standard interface. Wind tunnel experiment is carried out with the prototyped GPEH and a built up SSHI circuit hardware. System-level circuit simulation is conducted based on the equivalent circuit model of the GPEH. The benefits of SSHI compared to standard circuit become more significant at a high wind speed. In the low wind speed range, SSHI circuits lose its advantage. In both experiment and simulation, P-SSHI confirms its superiority over the standard circuit. A power increase of 43.75% is obtained with P-SSHI compared to the standard circuit, boosting the power output from 1.6mW to 2.3mW. While for S-SSHI, though the advantage is predicted by simulation, it is not confirmed yet in experiment. The discrepancies of S-SSHI need further investigation in the future work.

REFERENCES

[1] Beeby, S. P., Tudor, M. J. and White, N. M., “Energy harvesting vibration sources for microsystems applications,” Measurement science and technology, 17, R175 (2006).

[2] Anton, S. R., Sodano, H. A., “A review of power harvesting using piezoelectric materials (2003–2006),” Smart Materials and Structures, 16, R1–R21 (2007).

[3] Zhou, S., Cao, J., Erturk, A. and Lin, J., “Enhanced broadband piezoelectric energy harvesting using rotatable magnets,” Applied Physics Letters, 102(17), 173901 (2013).

[4] Tang, L., Yang, Y. and Soh, C. K., “Broadband vibration energy harvesting techniques,” Advances in Energy Harvesting Methods. Springer, 17-61 (2013).

[5] Priya, S., “Modeling of electric energy harvesting using piezoelectric windmill,” Applied Physics Letters, 87(18), 184101 (2005).

[6] Karami, M. A., Farmer, J. R. and Inman, D. J., "Parametrically excited nonlinear piezoelectric compact wind turbine," Renewable Energy, 50, 977-987 (2013).
[7] Akaydin, H. D., Elvin, N. and Andreopoulos, Y., "The performance of a self-excited fluidic energy harvester," Smart Materials and Structures, 21, 025007 (2012).
[8] Tam Nguyen, H. D., Pham, H. T. and Wang, D. A., "A miniature pneumatic energy generator using Kármán vortex street," Journal of Wind Engineering and Industrial Aerodynamics, 116, 40-48 (2013).
[9] Sirohi, J. and Mahadik, R., "Piezoelectric wind energy harvester for low-power sensors," Journal of Intelligent Material Systems and Structures, 22, 2215-2228 (2011).
[10] Abdelkefi, A., Yan, Z. and Hajj, M. R., "Modeling and nonlinear analysis of piezoelectric energy harvesting from transverse galloping," Smart Materials and Structures, 22, 025016 (2013).
[11] Yan, Z. and Abdelkefi, A., "Nonlinear characterization of concurrent energy harvesting from galloping and base excitations," Nonlinear Dynamics, 77(4), 1171-1189 (2014).
[12] Yang, Y., Zhao, L. and Tang, L., "Comparative study of tip cross-sections for efficient galloping energy harvesting," Applied Physics Letters, 102, 064105 (2013).
[13] Zhao, L., Tang, L. and Yang, Y., "Comparison of modeling methods and parametric study for a piezoelectric wind energy harvester," Smart Materials and Structures, 22, 125003 (2013).
[14] Zhao, L., Tang, L. and Yang, Y., "Enhanced piezoelectric galloping energy harvesting using 2 degree-of-freedom cut-out cantilever with magnetic interaction," Japanese Journal of Applied Physics, 53, 060302 (2014).
[15] Bibo, A., Abdelkefi, A. and Daqaq, M. F., "Modeling and characterization of a piezoelectric energy harvester under Combined Aerodynamic and Base Excitations," Journal of Vibration and Acoustics, doi:10.1115/1.4029611 (2015).
[16] Bryant, M. and Garcia, E., "Modeling and testing of a novel aeroelastic flutter energy harvester," Journal of Vibration and Acoustics, 133, 011010 (2011).
[17] De Marqui, C. and Erturk, A., "Electroaeroelastic analysis of airfoilbased wind energy harvesting using piezoelectric transduction and electromagnetic induction," Journal of Intelligent Material Systems and Structures, 24, 846-854 (2013).
[18] Bibo, A. and Daqaq, M., "Investigation of concurrent energy harvesting from ambient vibrations and wind using a single piezoelectric generator," Applied Physics Letters, 102, 243904 (2013).
[19] Bibo, A., Li, G. and Daqaq, M. F., "Performance analysis of a harmonica-type aeroelastic micropower generator," Journal of Intelligent Material Systems and Structures, 23, 1461-74 (2012).
[20] Hobeck, J. D. and Inman, D. J., "Artificial piezoelectric grass for energy harvesting from turbulence-induced vibration," Smart Materials and Structures, 21(10), 105024 (2012).
[21] Weinstein, L. A., Cacan, M. R., So, P. M. and Wright, P. K., "Vortex shedding induced energy harvesting from piezoelectric materials in heating, ventilation and air conditioning flows," Smart Materials and Structures, 21(4), 045003 (2012).
[22] Zhao, L. and Yang, Y., "Enhanced aeroelastic energy harvesting with a beam stiffener," Smart Materials and Structures, (2015) (accepted for publication).
[23] Badel, A., Guyomar, D., Lefeuvre, E. and Richard, C., "Piezoelectric energy harvesting using a synchronized switch technique," Journal of Intelligent Material Systems and Structures, 17, 831-39 (2006).
[24] Shu, Y., Lien, I. and Wu, W., "An improved analysis of the SSHI interface in piezoelectric energy harvesting," Smart Materials and Structures, 16, 2253 (2007).
[25] Lefeuvre, E., Badel, A., Richard, C. and Guyomar, D., "Energy harvesting using piezoelectric materials: Case of random vibrations," Journal of Electroceramics, 19, 349-355 (2007).
[26] Lallart, M. and Guyomar, D., "An optimized self-powered switching circuit for non-linear energy harvesting with low voltage output," Smart Materials and Structures, 17, 035030 (2008).
[27] Wu, W., Wickenheiser, A., Reissman, T. and Garcia, E., "Modeling and experimental verification of synchronized discharging techniques for boosting power harvesting from piezoelectric transducers," Smart Materials and Structures, 18, 055012 (2009).
[28] Liang, J. R. and Liao, W. H., "On the influence of transducer internal loss in piezoelectric energy harvesting with SSHI interface," Journal of Intelligent Material Systems and Structures, 22(5), 503-512 (2011).
[29] Liang, J. and Liao, W. H., "Improved design and analysis of self-powered synchronized switch interface circuit for piezoelectric energy harvesting systems," IEEE Transactions on Industrial Electronics, 59, 1950-1960 (2012).
[30] Tan, Y. K. and Panda, S., "Optimized wind energy harvesting system using resistance emulator and active rectifier for wireless sensor nodes," IEEE Transactions on Power Electronics, 26, 38–50 (2011).

[31] Bryant, M., Schlichting, A. D. and Garcia, E., "Toward efficient aeroelastic energy harvesting: device performance comparisons and improvements through synchronized switching," Proc. SPIE, 8688, 868807 (2013).
[32] Zhao, L., Tang, L., Wu, H. and Yang, Y., "Synchronized Charge Extraction for Aeroelastic Energy Harvesting," Proc. SPIE, 9057, 90570N (2014).
[33] Zhao, L., Tang, L. and Yang, Y., "Synchronized charge extraction in galloping piezoelectric energy harvesting," Journal of Intelligent Material Systems and Structures, (2015) (in press).
[34] Tang, L., Zhao, L., Yang, Y. and Lefeuvre, E., "Equivalent circuit representation and analysis of galloping-based wind energy harvesting," IEEE/ASME Transactions on Mechatronics, 20, 834-844 (2015).
[35] Elvin, N. G., "Equivalent electrical circuits for advanced energy harvesting," Journal of Intelligent Material Systems and Structures, 25(14), 1715–1726 (2014).
[36] Richard, C., Guyomar, D. and Lefeuvre, D., "Self-powered electronic breaker with automatic switching by detecting maxima or minima of potential difference between its power electrodes," Patent PCT/FR2005/003000 (publication number: WO/2007/063194) (2007).